atmosphere

MDPI

Article

A BVOC Emission Inventory for China in 2023 and Its Impacts on Ozone and Secondary Organic Aerosol Formation

Huiying Xu [1], Jiani Zhang [1], Yuqing Chen [1], Yian Zhou [1], Feiyang Qiao [1], Haomin Huang [1,2,3], Liya Fan [1,2,3] and Daiqi Ye [1,2,3,*]

[1] School of Environment and Energy, South China University of Technology, Guangzhou 510006, China; 202321048107@mail.scut.edu.cn (H.X.); esjianizhang@mail.scut.edu.cn (J.Z.); 202321047589@mail.scut.edu.cn (Y.C.); 202420146791@mail.scut.edu.cn (Y.Z.); 202420146771@mail.scut.edu.cn (F.Q.); huanghm@scut.edu.cn (H.H.); fanly@scut.edu.cn (L.F.)
[2] Guangdong Provincial Key Laboratory of Atmospheric Environment and Pollution Control, Guangzhou 510006, China
[3] National Engineering Laboratory for VOCs Pollution Control Technology and Equipment, South China University of Technology, Guangzhou 510006, China
* Correspondence: cedqye@scut.edu.cn

Abstract

Volatile organic compounds (VOCs) are key precursors of ozone (O_3) and secondary organic aerosols (SOA), among which biogenic VOCs (BVOCs) constitute the dominant natural source. However, large uncertainties remain in the magnitude, spatial distribution, and seasonal variability of BVOC emissions in China under rapidly changing vegetation and climate conditions. In this study, a refined BVOC emission inventory for China in 2023 was developed using the Model of Emissions of Gases and Aerosols from Nature (MEGAN v3.2) driven by WRF meteorological simulations and MODIS vegetation data. The estimated annual BVOC emissions reached 41.70 Tg, including 26.90 Tg isoprene, 4.84 Tg monoterpenes, 0.55 Tg sesquiterpenes, and 9.41 Tg other VOCs. The corresponding ozone formation potential (OFP) and secondary organic aerosol formation potential (SOAFP) were 346.12 Tg yr^{-1} and 2137.51 Gg yr^{-1}, respectively. Emissions exhibited a pronounced south–north gradient with hotspots in Guangxi, Guangdong, and Yunnan, and peaked in summer. Broadleaf forests were identified as the dominant emission sources, followed by savannas and shrublands. Isoprene contributed most to OFP, whereas monoterpenes dominated SOAFP. Compared with previous inventories, the updated vegetation data, meteorological inputs, and refined chemical speciation improve the representation of BVOC emissions and their spatial patterns in China. These results highlight the important role of BVOCs in regional O_3 and SOA formation and provide an improved emission basis for atmospheric chemistry modeling and air-quality management.

Keywords: biogenic volatile organic compounds; Emission inventory; MEGAN v3.2; China

Academic Editor: Iustinian Gabriel Bejan

Received: 8 March 2026
Revised: 31 March 2026
Accepted: 4 April 2026
Published: 10 April 2026

1. Introduction

Air pollution remains a persistent environmental challenge in China, with high levels of ozone (O_3) and fine particulate matter ($PM_{2.5}$) frequently exceeding national air-quality standards. A major contributor to these pollutants is the atmospheric oxidation of volatile organic compounds (VOCs), which drive the formation of both O_3 and secondary organic aerosols (SOA) [1–3]. Among VOCs, biogenic VOCs (BVOCs) emitted from terrestrial vegetation represent the dominant natural component, accounting for more than two-thirds

of global VOC emissions [4–7]. BVOCs include isoprene, monoterpenes, sesquiterpenes, and other species include methanol, acetone, and ethene, etc., which are highly reactive and strongly influence regional air quality and climate processes [8,9].

Accurate representation of BVOC emissions is essential for improving air-quality simulations and guiding anthropogenic source management [10,11]. Reliable models depend on precise natural emission inputs, as errors in BVOC estimates can propagate through photochemical mechanisms, leading to large uncertainties in simulated O_3 and SOA concentrations [3,10–12]. Moreover, China's carbon neutrality targets and large-scale afforestation programs have important implications for BVOC emissions. Expanding vegetation coverage increases natural VOC sources, which can interact with decreasing anthropogenic emissions to influence summertime O_3 and SOA formation [13,14]. Therefore, the development of robust, data-driven BVOC emission inventories is a key prerequisite for effective air-quality control and scientific policy formulation in China.

However, existing BVOC inventories for China exhibit substantial inconsistencies, with reported annual totals ranging from 10 to nearly 60 Tg yr^{-1} [11,15–19]. These discrepancies arise primarily from the use of global-average emission factors that overlook China's diverse vegetation composition, outdated or coarse-resolution land-cover datasets, and simplified model algorithms that poorly capture local meteorological dynamics [16,20–22]. In addition, deficient model algorithms and input data in previous studies have introduced large uncertainties, and current national inventories may underestimate BVOC emissions in China [23]. These uncertainties limit the ability to accurately quantify the contribution of BVOCs to O_3 and SOA pollution in China.

To address these limitations, this study develops a chemically detailed BVOC emission inventory for China for the year 2023. The inventory is generated using the latest version of the Model of Emissions of Gases and Aerosols from Nature (MEGAN v3.2) coupled with the Weather Research and Forecasting (WRF v3.8.1) model. The modeling framework integrates satellite-based vegetation and land surface information to capture spatial heterogeneity and seasonal dynamics under real meteorological conditions. This updated framework enables the estimation of hourly BVOC emissions at 36 km $\times$ 36 km resolution, resolving isoprene, monoterpenes, sesquiterpenes, and other VOCs (OVOCs) as well as their subcategories. Furthermore, the inventory quantifies both O_3 formation potential (OFP) and SOA formation potential (SOAFP), providing a comprehensive assessment of BVOC contributions to air pollution. By incorporating improved model algorithms, updated input data, and refined chemical speciation, this study substantially reduces uncertainties in previous inventories and offers new insights into the magnitude, spatial distribution, and atmospheric impacts of BVOC emissions in China, supporting the formulation of policies that balance carbon neutrality goals with air quality management.

2. Methodology and Data

2.1. MEGANv3.2

The MEGAN is a widely applied tool for simulating BVOC emissions at both global and regional scales [24] and has been incorporated into numerous Earth system and chemical transport models [25]. In this study, we apply MEGANv3.2 to estimate BVOC emissions, which improves upon MEGANv2.1 by deriving emission factors (EFs) using its emission factor processor (EFP) rather than relying solely on fixed plant functional types (PFTs). The EFP integrates: (1) plant growth forms (trees, shrubs, grasses, crops), defined as the broad structural category of vegetation used by MEGAN to represent canopy architecture and functional structure; (2) ecotype datasets combining species with distinct emission potentials; and (3) updated species-level emission factor datasets compiled from

over 10,000 measurements [26]. These improvements allow differentiation of emission factors across regions sharing the same PFT but with distinct vegetation compositions.

In addition, MEGANv3.2 expands the number of chemical species from 148 to more than 200, and incorporates additional stress functions including extreme temperature, strong wind, and O_3 stress. The model estimates the BVOC emission rate (ER) as shown in Equation (1):

$$ER = EF \times EA \quad (1)$$

where EF is the standard emission factor under reference conditions and EA is the nondimensional activity factor. The EF for each grid cell is calculated as a weighted average of the four plant growth forms, according to Equation (2):

$$EF = EF_{tree} \times f_{tree} + EF_{shrub} \times f_{shrub} + EF_{grass} \times f_{grass} + EF_{crop} \times f_{crop} \quad (2)$$

where EF_{tree}, EF_{shrub}, EF_{grass}, EF_{crop} denote the emission factors of the four growth forms, and f represents their fractional cover within each grid cell.

The emission activity factor EA accounts for environmental modulation, is expressed in Equation (3):

$$EA = LAIv \times \gamma_P \times \gamma_T \times \gamma_{HT} \times \gamma_{LT} \times \gamma_{SW} \times \gamma_{O_3} \times \gamma_A \times \gamma_{SM} \times \gamma_C \quad (3)$$

where LAIv is the vegetation-covered leaf area index, and γ terms represent response functions to radiation, temperature, heat/cold stress, wind, O_3, leaf age, soil moisture, and CO_2 concentration. In MEGANv3.2, higher temperature, radiation, and soil moisture enhance BVOC emissions, whereas extreme heat (>43 °C), cold (<6 °C), strong wind (>12 m s^{-1}), and elevated O_3 (>40 ppb) suppress emissions. CO_2 inhibition currently applies only to isoprene [25–27]. The empirical thresholds and response curves for these stress factors follow Guenther et al. (2020) [26] and are incorporated in the model by multiplying the corresponding γ factors with the base emission rate.

2.2. Data

The input datasets for MEGANv3.2 simulations were derived from meteorological fields and satellite-based vegetation products. Meteorological parameters were generated using WRF v3.8.1, a widely used model for high-resolution dynamical downscaling [28,29]. The model provides hourly gridded variables, including surface air temperature, downward shortwave radiation (DSR), wind speed, and soil moisture, which are used in emission activity factor calculations in MEGAN.

The reliability of the WRF-simulated meteorological fields was evaluated using two key variables: 2 m air temperature (T_{2m}) and DSR. Observed T_{2m} data from 411 sites were obtained from the National Centers for Environmental Information (NCEI) [30], while DSR data were derived from the China Meteorological Forcing Dataset v2.0 (CMFD) [31], which integrates ERA5 reanalysis and ground observations. Statistical results (Tables S1 and S2; Figures S1 and S2) show high correlation coefficients (R = 0.97 for T_{2m} and 0.98 for DSR) and low biases (−1.32 °C for T_{2m} and 7.01 W m^{-2} for DSR), indicating that WRF reasonably reproduces temperature and radiation patterns across China. The spatial distributions of T_{2m} and DSR in 2023 are shown in Figure 1, providing a spatial basis for interpreting BVOC emission variability.

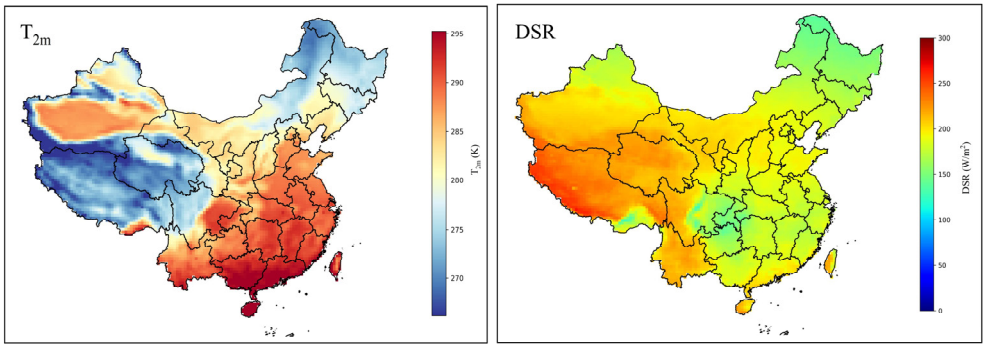

Figure 1. Spatial distribution of T_{2m} and DSR from WRF Simulations over China in 2023.

Vegetation inputs were derived from Moderate Resolution Imaging Spectroradiometer (MODIS) products, which provide long-term, globally consistent observations and are used to characterize vegetation structure and composition in MEGAN v3.2 [32,33]. The MCD15A2H v061 product provides leaf area index (LAI) at 8-day temporal and 500 m spatial resolution [34], which is a key variable controlling canopy-level BVOC emissions [35]. To better represent the effective emitting canopy, LAI was combined with vegetation continuous fields (VCF) to derive vegetation-covered LAI (LAIv), accounting for fractional vegetation cover within each grid cell. The MOD44B v061 product provides annual VCF at 250 m resolution, describing the fractional cover of trees, shrubs, and grasses [36]. In addition, the MCD12Q1 v061 dataset provides annual land-cover and PFT classifications at 500 m resolution [37], which are used to represent vegetation type distribution and provide inputs for the MEGAN EFP. All datasets were resampled to the 36 km × 36 km WRF grids using area-weighted averaging. Together, these datasets constrain the spatial variability of BVOC emission potentials in MEGAN v3.2.

2.3. O_3 and SOA Formation Potentials

To evaluate the atmospheric impacts of BVOC emissions, both the O_3 formation potential (OFP) and the SOA formation potential (SOAFP) were quantified in this study. The OFP of each species was calculated using the maximum incremental reactivity (MIR), and the SOAFP was calculated using the fractional aerosol coefficient (FAC). These two indicators are emission-based metrics that provide insights into the relative contribution of individual BVOC species to O_3 and aerosol formation, respectively [38]. It should be noted that these metrics estimate the potential formation based on standardized coefficients, and do not explicitly simulate the depletion of O_3 or the dynamic partitioning of organic aerosol under real atmospheric conditions. Therefore, the absolute magnitude of O_3 or SOA formation may differ under variable meteorology, oxidant availability, or urban pollution levels. The actual atmospheric outcomes can be further assessed using detailed air quality models.

The OFP of each BVOC species is calculated as shown in Equation (4):

$$OFP_{i,j} = E_{i,j} \times MIR_j \quad (4)$$

where $OFP_{i,j}$ represents the O_3 formation potential of VOC species j from source i (g O_3 yr^{-1}), $E_{i,j}$ is the annual emission of species j from source i (g $BVOC_j$ yr^{-1}), and MIR_j (g O_3 g^{-1} $BVOC_j$) denotes the maximum incremental reactivity coefficient of that species. The MIR values adopted in this study were obtained from previous literature sources [39].

Similarly, the SOAFP is estimated for each BVOC species according to Equation (5):

$$SOAFP_{i,j} = E_{i,j} \times FAC_j \quad (5)$$

where $SOAFP_{i,j}$ is the SOA formation potential of VOC species j from source i (g SOA yr^{-1}), $E_{i,j}$ represents the emission of species j from source i (g $BVOC_j$ yr^{-1}), and FAC_j (g SOA g^{-1} $BVOC_j$) is the fractional aerosol coefficient, reflecting the tendency of species j to form SOA under atmospheric conditions. The FAC values were compiled from several published studies [40–42].

By applying both OFP and SOAFP metrics, this study provides a more comprehensive assessment of the role of BVOC emissions in driving tropospheric O_3 production and SOA formation. These metrics serve as a first-order evaluation of BVOC impacts across regions and species, highlighting the relative importance of different precursors while acknowledging that actual atmospheric responses may be influenced by additional chemical and meteorological factors.

2.4. Uncertainty Analysis of the Emission Inventory

The uncertainty of simulated BVOC emissions was quantified using a Monte Carlo approach, which has been widely employed in uncertainty assessments of emission inventories [43–45]. Monte Carlo simulation is a probabilistic numerical method in which input parameters are randomly sampled according to their prescribed probability distributions, and the corresponding model outputs are calculated based on the functional relationships between inputs and outputs. By repeating this process a large number of times (typically on the order of 10^5–10^6 iterations), a probability distribution of the target variable can be constructed, allowing the uncertainties of input parameters to be propagated to the model results. The 2.5th and 97.5th percentiles of the resulting distribution are commonly used to define the 95% confidence interval [44]. In this study, the Monte Carlo framework was applied to quantify the uncertainty in the BVOC emission inventory. The probability distributions of key input parameters were specified as follows: uncertainties in EFs were derived from observational studies of native vegetation in China [43]; uncertainties associated with vegetation parameters and key empirical coefficients in the MEGAN model were adopted from Situ et al. (2014) [45]; and uncertainties in meteorological driving variables were constrained based on the discrepancies between WRF simulations and observational data evaluated in this study. Based on these prescribed distributions, 10,000 random simulations were conducted, and the resulting BVOC emissions were expressed in terms of a 95% confidence interval.

3. Results and Discussion

3.1. Comparison of Model Emission Estimates with Flux Measurements

The BVOC emission inventory was evaluated against field observations of BVOC fluxes reported in previous studies across China [46–48]. Due to the lack of observations for 2023, simulations were conducted for the corresponding observational periods using the same modeling framework to ensure temporal consistency. BVOC emissions were extracted from grid cells corresponding to each observation site and compared directly with measured fluxes, based on 82 observational data points. Model performance was quantitatively assessed using statistical metrics, including the R, mean bias (MB), mean absolute error (MAE), and root mean square error (RMSE). The results show a moderate correlation between simulated and observed values (Figure 2), with a correlation coefficient R of 0.61, indicating that the model reasonably captures the variability of BVOCs emissions. The MB is −0.11, suggesting a slight overall underestimation. Meanwhile, the mean absolute error MAE of 0.13 and the root mean square error RMSE of 0.23 remain relatively low, demonstrating that the overall simulation errors are within an acceptable range.

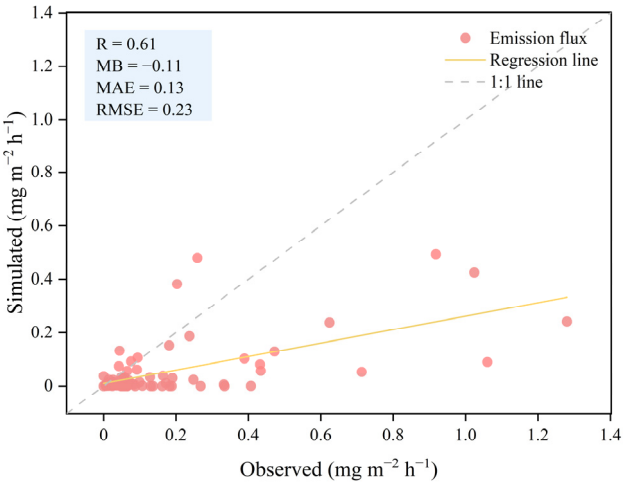

Figure 2. Comparison between observed and simulated BVOCs fluxes across China.

3.2. Emissions and Composition

In 2023, the national annual BVOC emission was 41.70 Tg, dominated by isoprene (26.90 Tg, 64%), followed by OVOCs (9.41 Tg, 23%), monoterpenes (4.84 Tg, 12%) and sesquiterpenes (0.55 Tg, 1%). The emission amounts and compositional contributions of different BVOC categories are illustrated in Figure 3. The prevalence of isoprene reflects the high emission potential of widely distributed vegetation types [49,50]. Within monoterpenes, α-pinene (1 972.14 Gg) and β-pinene (682.35 Gg) were the largest contributors, while β-caryophyllene (127.62 Gg) and α-farnescene (121.19 Gg) dominated the sesquiterpene. In the OVOCs class, methanol and acetone accounted for the largest shares (51% and 12%, respectively). The top ten BVOC species in 2023 were isoprene, methanol, α-pinene, acetone, β-pinene, acetaldehyde, ethanol, ethene, β-ocimene, and limonene, which collectively accounted for 91% of the total BVOC emissions, representing the majority of the national BVOC emissions.

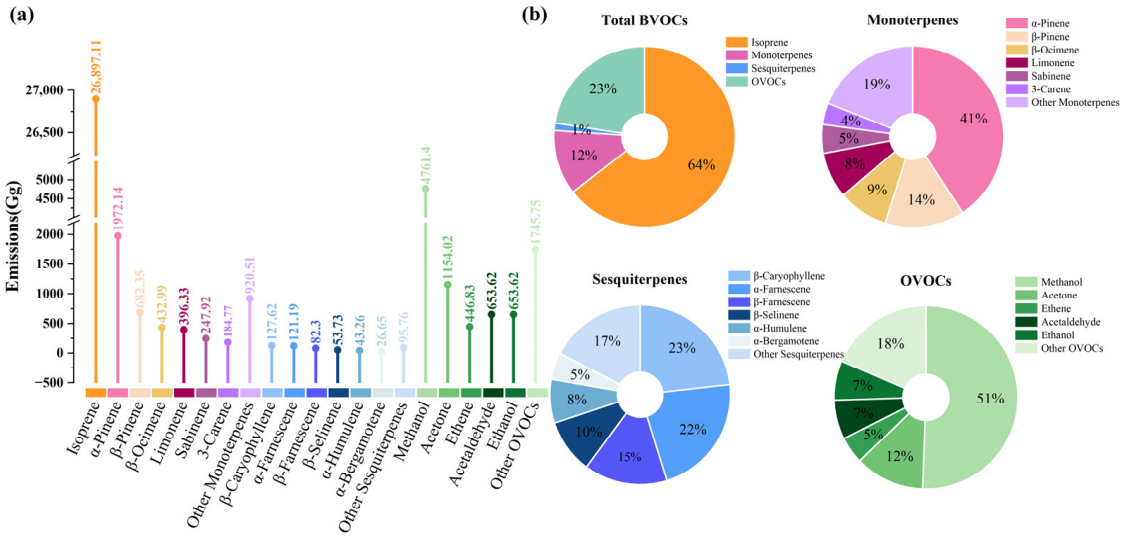

Figure 3. Contributions of BVOC species in China in 2023: (**a**) emissions of major compounds and (**b**) composition of each compound class.

The total emission estimated in this study (41.70 Tg) lies within the range of previous results (15.66–53.5 Tg) derived from different versions of MEGAN using various meteorological and vegetation datasets [11,15–19] (Table S3). Compared with earlier studies, isoprene emissions in this work are relatively higher, whereas monoterpene and OVOCs

emissions are lower. The differences mainly arise from the following: (1) Model version updates: MEGANv3.2 uses updated, species-specific emission factors and improved vegetation representation beyond the PFT-based scheme in MEGANv2.1, enhancing isoprene estimates and refining monoterpene and OVOC calculations [26]. (2) Vegetation data resolution and coverage: The use of high-resolution 2023 MODIS vegetation and LAI datasets better captures spatial heterogeneity than earlier datasets (e.g., Vegetation Atlas of China). (3) Emission factor updates: Updated EFs in MEGANv3.2 reflect recent field data, reducing uncertainties compared with earlier generalized values [26]. (4) Meteorological variability: The 2023 emissions were influenced by temperature, shortwave radiation, and other meteorological drivers, which differ from years in previous studies. Elevated temperatures or higher solar radiation can enhance isoprene emissions significantly, explaining part of the increase relative to earlier inventories. These comparisons indicate that model version, vegetation data, emission factors, and meteorological conditions are the main sources of inter-study differences.

Although this study focuses on the 2023 BVOC emission inventory, a multi-year dataset (2019–2023) was analyzed to assess its representativeness (Figure 4). Over this period, total BVOC emissions increased from 33.19 Tg to 41.70 Tg, with 2023 representing the highest emission level in recent years. This increase reflects the combined influence of meteorological variability and vegetation dynamics. Interannual changes in temperature, solar radiation, and precipitation modulate emission rates, particularly for isoprene and monoterpenes, while increasing vegetation coverage—driven by afforestation and land-use policies—has expanded the distribution of high-emission vegetation types. Despite these variations in total emission magnitude, the relative composition of BVOC species and their spatial distribution patterns remain largely stable across years. Isoprene consistently dominates the emission profile (62–65%), while monoterpenes and OVOCs exhibit limited variability and sesquiterpenes contribute only a minor fraction (1%). This structural stability indicates that interannual variability mainly affects emission intensity rather than emission patterns. Therefore, the selection of 2023 is not only representative of recent BVOC emission characteristics but also corresponds to a period of relatively elevated emissions under current climatic and ecological conditions.

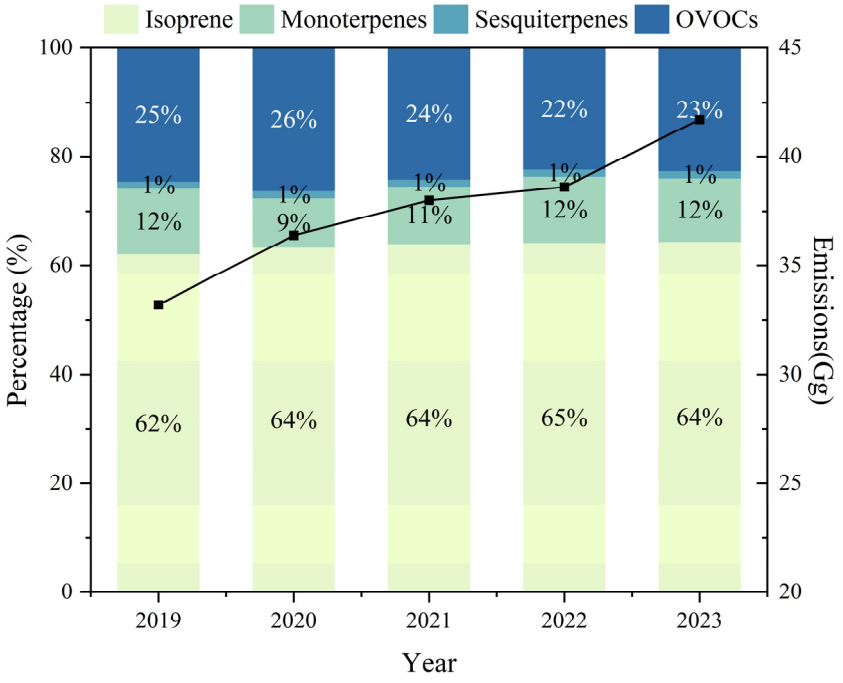

Figure 4. Annual BVOC emissions and composition in China from 2019 to 2023.

3.3. Sources of BVOC

Isoprene is the dominant BVOC species in China, accounting for 65% of total emissions, and is mainly released from broadleaf forests (75%) (Figure 5a). Its high abundance reflects the widespread distribution of isoprene-emitting vegetation and the strong photosynthetic activity of broadleaf species. Isoprene is synthesized de novo during photosynthesis and emitted instantaneously, allowing plants to mitigate oxidative stress under high light and temperature conditions [51,52]. Monoterpenes contribute 12% of the total BVOC budget, with α-pinene and β-pinene as the dominant components. These compounds are primarily emitted by coniferous forests (~40%), where they are stored in resin ducts and released through storage-based pathways that sustain fluxes even under low radiation [53,54]. Broadleaf forests emit only small fractions of monoterpenes (<10%) because they lack such specialized storage tissues. Sesquiterpenes represent a smaller fraction of total emissions (1%), but their key species, β-caryophyllene and α-farnescen, are mainly released from broadleaf forests and shrublands. Their emissions are typically associated with secondary metabolic activity and stress responses such as heat, radiation, and tissue damage [54–56]. OVOCs account for 23% of total BVOC emissions, dominated by methanol and acetone. High OVOC emissions occur in savannas and grasslands, largely due to rapid herbaceous turnover and active cellular metabolism that promote the release of oxygenated compounds [56]. They are mainly produced through plant metabolic activity and stress responses, while in croplands, elevated OVOC emissions are also associated with agricultural disturbances such as harvesting and biomass burning [57].

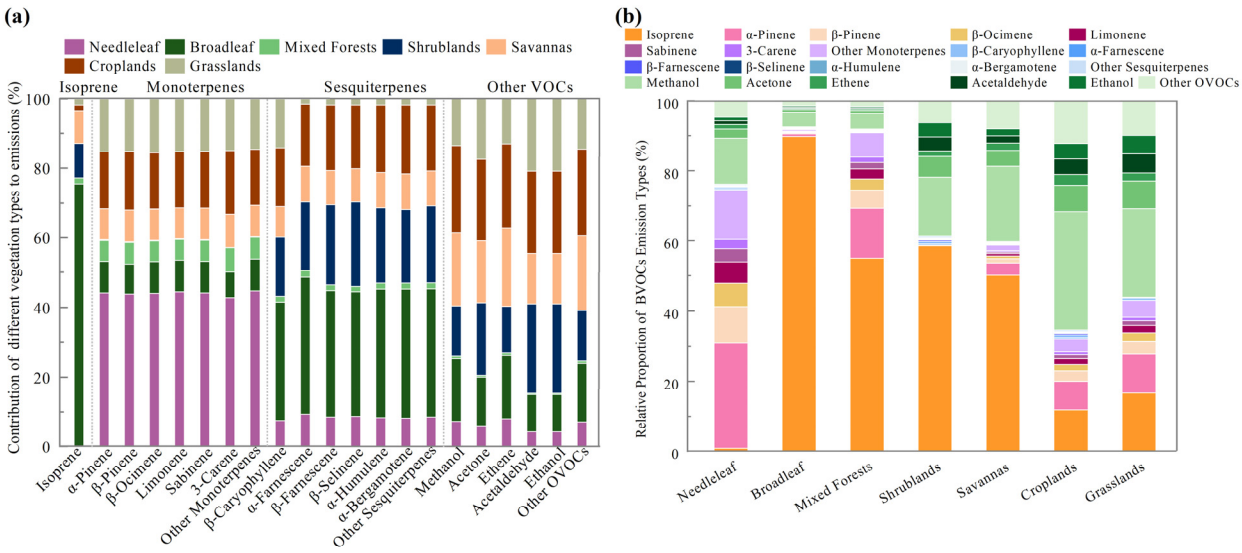

Figure 5. Vegetation sources of BVOC emissions in China: (**a**) contributions of different vegetation types to major BVOC emissions, and (**b**) BVOC composition profiles of each vegetation type.

Different vegetation types exhibit distinct BVOC profiles shaped by physiological traits, LAI, and vegetation cover. Nationally, broadleaf forests are the dominant source, contributing 53% of total BVOC emissions, followed by savannas (12%), shrublands (10%), croplands (9%), grasslands (7%), needleleaf forests (7%), and mixed forests (2%). As shown in Figure 5b, needleleaf forests are strongly monoterpene-dominated (74%), with minimal isoprene, sesquiterpene, and OVOCs emissions, reflecting resin storage and stress resistance [53]. In contrast, broadleaf forests are overwhelmingly isoprene-driven (90%), followed by OVOCs, while monoterpenes and sesquiterpenes each contribute less than 10%. This pattern reflects light- and temperature-driven isoprene synthesis in broadleaf foliage, whereas OVOCs mainly originate from cell wall expansion, metabolic activity, and stress

responses [54–56]. Mixed forests, with overall low BVOC emission levels and contributing less than 2% nationally, primarily release isoprene and monoterpenes. Their emission characteristics are associated with the mixed composition of needleleaf and broadleaf forests and the relatively complex canopy structure. Shrublands and savannas are both dominated by isoprene and OVOCs, though shrublands show relatively more isoprene, while savannas present a transitional profile combining herbaceous OVOCs emissions with woody isoprene release. Croplands and grasslands are characterized by OVOCs dominance (65% and 56%, respectively), with isoprene accounting for 12% in croplands and 17% in grasslands, and monoterpenes contributing 20% and 26%, respectively. Sesquiterpenes remain limited in both systems.

3.4. Spatial Distribution

Figure 6a shows the spatial distribution of BVOC emissions in China for 2023. Emissions display distinct regional heterogeneity, controlled by vegetation cover and climatic conditions. High emissions occur in southeastern and northeastern China, southern Shaanxi, eastern Sichuan, Hainan, and Taiwan, where grid-level emissions exceed 60 Gg yr^{-1} in some areas. The overall pattern shows a clear southeast–northwest gradient, with much lower values over the arid and sparsely vegetated northwestern plateau. According to the MODIS PFT distribution (Figure S3) and vegetation area statistics (Table S4), southeastern provinces such as Guangxi, Guangdong, Fujian, and Hunan have extensive broadleaf forests (35,000–37,000 km^2) and large areas of savannas (over 60,000 km^2). Broadleaf forests are identified as the dominant vegetation source, contributing 53% of total BVOC emissions. They overwhelmingly control isoprene emissions, accounting for 75% of the total. The elevated emissions in southeastern China result mainly from the large extent of broadleaf forests and the warm, humid climate, which enhances light- and temperature-driven emissions of isoprene and other terpenes [56]. In particular, regions such as Guangdong and Guangxi exhibit both high near-surface temperatures (T_{2m} > 295 K) and relatively strong solar radiation according to WRF simulations (Figure 1), jointly favoring higher emission rates. In contrast, the North China Plain, though rich in croplands with high LAI, emits less isoprene because the major crops (e.g., wheat and maize) have low isoprene emission potentials under comparable environmental conditions [58], and local temperature and radiation levels are not as favorable as in southern regions.

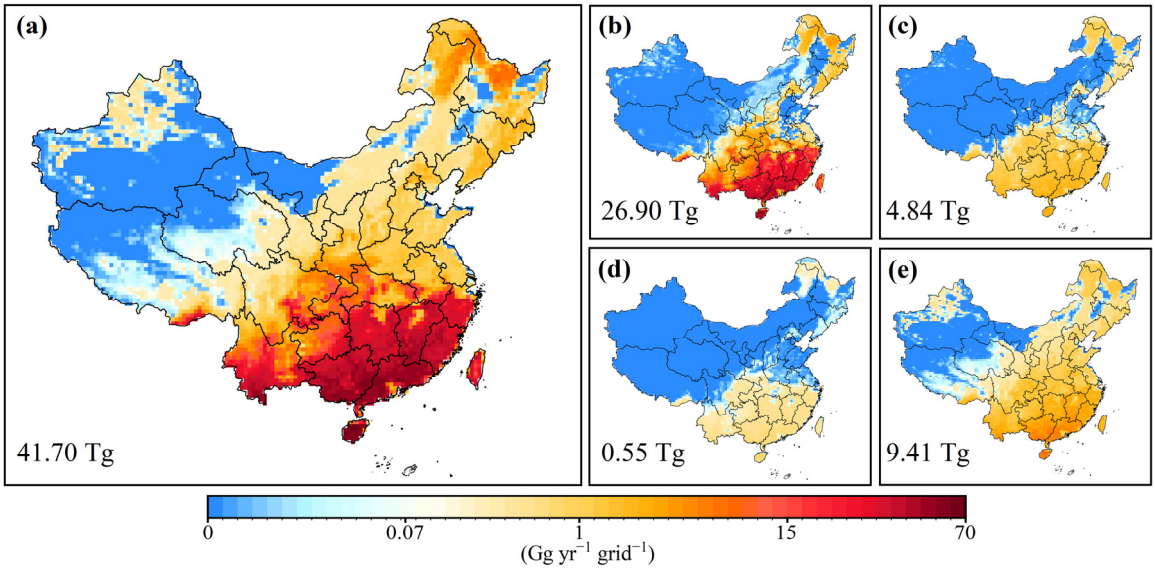

Figure 6. Spatial distribution of BVOC emissions in China for 2023. (**a**) Total BVOC emissions; (**b**) isoprene; (**c**) monoterpenes; (**d**) sesquiterpenes; (**e**) OVOCs.

Figure 6b–e presents the spatial distribution of different BVOC categories. Isoprene emissions are concentrated in South and Southeast China, particularly in Guangxi, Guangdong, Hunan, Fujian, Zhejiang, Hainan, and Taiwan, corresponding to regions with broadleaf forests and savannas covering more than 60% of land area (Table S4). These regions also feature higher near-surface temperatures and solar radiation (Figure 1), which favor isoprene release. Monoterpenes show a bimodal pattern: one maximum in Northeast China (Greater and Lesser Khingan Ranges, Changbai Mountains) dominated by coniferous forests, and another in the subtropical south where evergreen and mixed forests are extensive. The southern maximum coincides with warm, humid conditions, whereas the northeastern peak mainly reflects vegetation control rather than temperature. Sesquiterpene emissions resemble monoterpenes but are weaker, with maximum grid values below 1 Gg yr^{-1}. Although their spatial correspondence reflects similar vegetation distributions, sesquiterpene emissions are constrained by metabolic competition with essential metabolites (e.g., sterols) and their highly inducible, resulting in relatively low regional contributions [59]. OVOCs are widely distributed except in arid northwest China, with higher fractions in southern coastal areas. These areas coincide with dense croplands and forests that enhance both direct OVOC release and secondary formation. In Northwest China, despite strong solar radiation, limited vegetation cover and dry conditions suppress BVOC emissions. In contrast, although total emissions are low in the north and northwest, the fractional contribution of OVOCs to total BVOCs is relatively high, indicating their importance under local vegetation and climatic conditions.

3.5. Provincial and Temporal Distribution

Figure 7a shows the spatial variability of BVOC emissions by province. Provinces were grouped into high-, medium-, and low-emission categories. In the figure, these categories are represented by a color gradient: blue for low, yellow for medium, and red for high emissions, with darker shades indicating higher emissions within each category. High-emission regions are mainly distributed in South, Southwest, and parts of East China, representing the national emission core. Moderate emissions appear in the middle and lower reaches of the Yangtze River, North China, and the northwest margins, while low-emission provinces are concentrated in arid and urbanized areas. Provincial totals (Figure 7b) show that Guangxi and Guangdong record the highest emissions (6940.35 and 5225.55 Gg yr^{-1}), consistent with their extensive forest cover and tropical climate. In contrast, Shandong, Beijing, and Xinjiang emit less than 200 Gg yr^{-1}, mainly due to cropland dominance and limited forested land, and cooler or drier climates that constrain biogenic activity. Hong Kong, Ningxia, Tianjin, and Shanghai contribute less than 30 Gg yr^{-1}, negligible in the national total. The vegetation composition pattern in Table S4 supports this gradient, confirming that provinces with extensive broadleaf forests and savannas, combined with elevated temperature and strong solar radiation (Figure 1), exhibit the highest BVOC fluxes. Regional differences are also evident in chemical composition. Southern provinces are dominated by isoprene, which generally contributes over 60% of total BVOC emissions, followed by monoterpenes and OVOCs. In the north and northwest, OVOCs and monoterpenes constitute a larger share, reflecting the dominance of herbaceous and shrub species and the influence of environmental stress on emission pathways. Overall, BVOC emissions in China show a clear "strong south–weak north, low west–high east" pattern, with distinct compositional contrasts among regions.

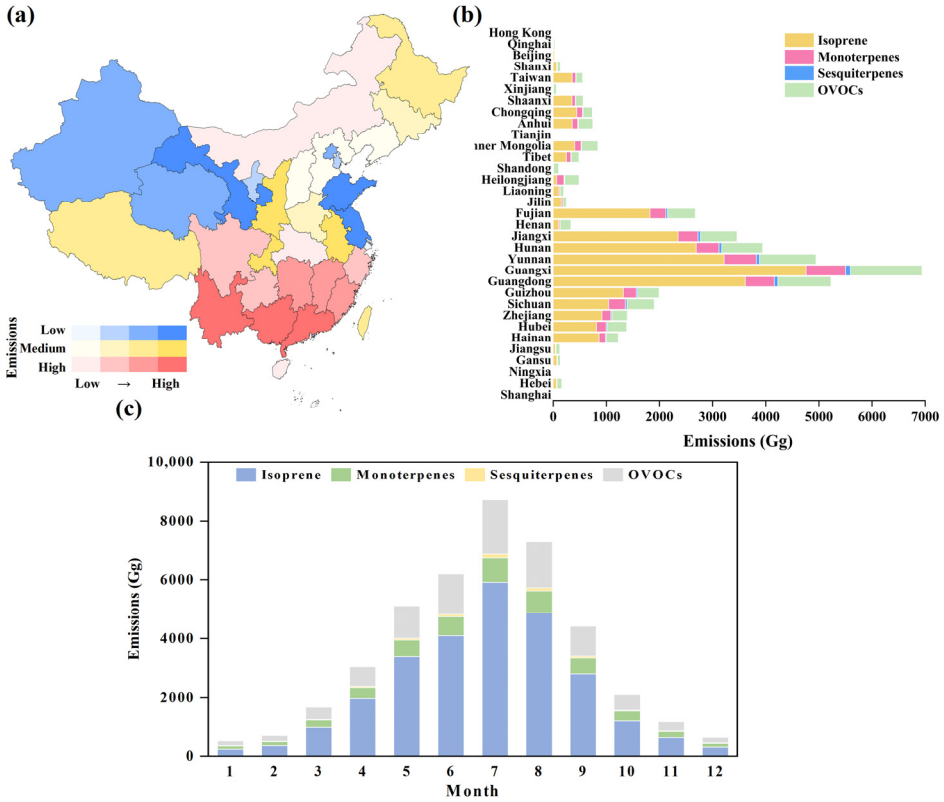

Figure 7. Provincial and seasonal characteristics of BVOC emissions in China. (**a**) Spatial distribution of provincial BVOC emissions; (**b**) total annual BVOC emissions for each province; (**c**) monthly variation of BVOC emissions at the national scale.

The monthly emission profile (Figure 7c) reveals pronounced seasonality. Emissions peak in summer and reach minima in winter, driven by vegetation activity and climatic factors. Isoprene shows the largest seasonal amplitude, with July emissions exceeding winter values by more than twentyfold. This pattern results from its strong dependence on temperature and radiation: high summer temperatures and sunlight stimulate isoprene synthase and increase precursor supply [50,54]. Seasonal variations in LAI further amplify this effect [49,50]. Leaf age is also an important factor regulating BVOC composition. According to MEGANv3.2, the isoprene emission potentials of newly developed and expanding leaves are only 5% and 60% of mature leaves, respectively, leading to relatively low emissions in spring. In autumn, senescing leaves exhibit a reduced emission potential of 90% relative to mature leaves, resulting in the characteristic "summer peak—spring/autumn transition—winter low" pattern for isoprene [15]. Monoterpenes and sesquiterpenes show seasonal patterns similar to isoprene, with higher emissions in summer and lower emissions in winter, but with smaller amplitudes. Their dependence on both temperature and diffusion, as well as partial storage within plant tissues, moderates seasonal fluctuations [53,60,61]. Leaf age also affects these emissions: monoterpene potentials of new, expanding, and senescent leaves reach about 200%, 180%, and 105% of mature leaves, respectively, while sesquiterpenes show 40–60% in young leaves and about 95% in senescent ones [15]. OVOCs also display clear seasonality, increasing in summer due to enhanced metabolic activity and temperature-driven volatilization, but with weaker variations than isoprene. In summary, the seasonal variability of BVOCs arises from differences among compounds in physiological metabolic pathways and emission mechanisms.

3.6. Impact on OFP

Figure 8 shows the spatial pattern of BVOC-driven OFP in China for 2023. The total OFP was 346.12 Tg. Isoprene dominated, contributing 285.38 Tg (82%), owing to both its large emissions (65%) and high reactivity (MIR = 10.61; see Table S5), underscoring its key role in O_3 formation. OVOCs and monoterpenes contributed 29.49 Tg (9%) and 27.00 Tg (8%), respectively. Within these groups, propene (MIR = 11.66) and α-pinene (MIR = 4.51) were the major species, accounting for 15% and 33% of their group totals. Sesquiterpenes contributed only 4.25 Tg (1%) to total OFP, consistent with their low emissions, though their high MIR values (5.55–12.82) suggest potential local importance under concentrated conditions. The ten leading species—namely isoprene, α-pinene, β-ocimene, propene, acetaldehyde, ethene, methanol, β-pinene, (Z)-3-hexenal, and myrcene—accounted for 93% of total OFP while representing 88% of total BVOC emissions. These results reveal a clear non-linear amplification effect, whereby a limited number of highly reactive species disproportionately control O_3 formation potential, highlighting that OFP is governed not only by emission magnitude but also by chemical reactivity weighting. Overall, isoprene overwhelmingly dominates the national O_3 formation potential, while monoterpenes and other highly reactive compounds such as propene and ethene make secondary but non-negligible contributions. These findings indicate that evaluating BVOC–O_3 relationships requires considering both emission magnitude and chemical reactivity.

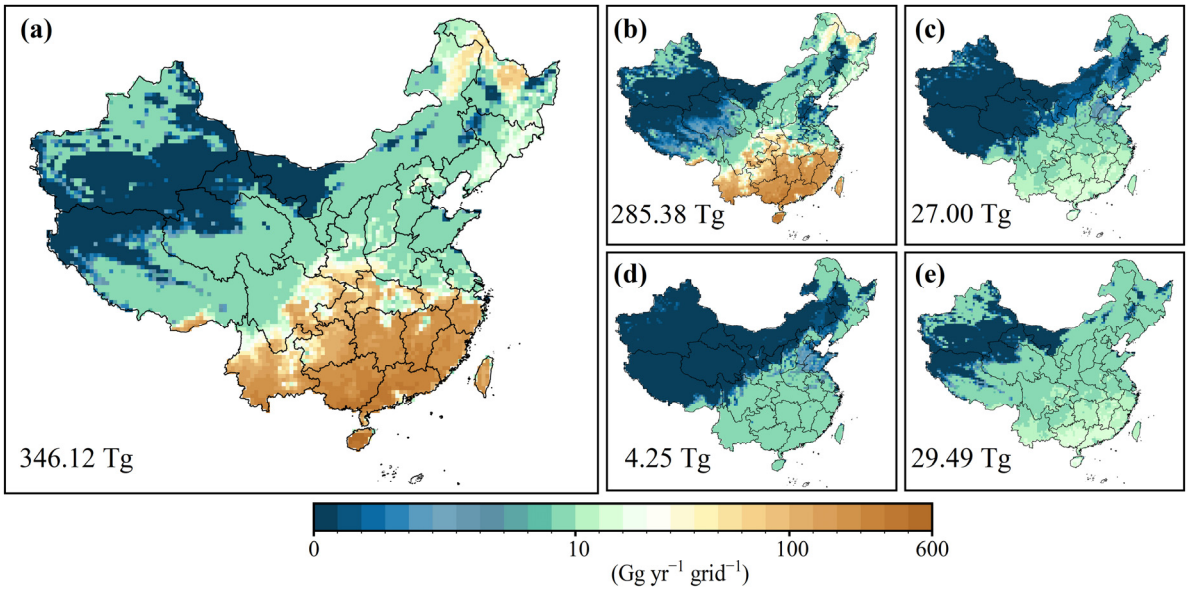

Figure 8. Spatial distribution of OFP from BVOC emissions in China for 2023. (**a**) Total OFP from BVOCs; (**b**) isoprene; (**c**) monoterpenes; (**d**) sesquiterpenes; (**e**) OVOCs.

OFP shows a spatial pattern similar to BVOC emissions, with a "high-south–low-north" gradient but sharper contrasts among provinces (Figure 9a). The highest values occur in Guangxi (50.50 Tg yr^{-1}), Yunnan (41.26 Tg yr^{-1}), and Guangdong (38.37 Tg yr^{-1}), jointly contributing over 30% of the national total. In these provinces, isoprene accounts for more than 85% of OFP. Central provinces such as Hunan, Jiangxi, and Hubei form a secondary high-value cluster, contributing around 21% of the total. Northern and northwestern provinces (e.g., Beijing, Tianjin, Hebei, Shanxi) exhibit low OFP levels, largely reflecting lower vegetation density and weaker isoprene activity. In these low-emission regions, OVOCs represent a larger proportion of the total despite low absolute values. Overall, southern provinces are dominated by isoprene-driven O_3 potential, whereas northern and arid regions show a higher relative share of OVOCs. However, it should be emphasized

that OFP, derived from MIR values, represents the theoretical maximum O_3 formation potential under idealized high-NOx conditions and does not directly correspond to actual ambient O_3 concentrations. In the real atmosphere, O_3 formation is governed by complex nonlinear photochemical processes involving the coupled interactions of VOCs, NOx, and radical species [62,63]. Specifically, BVOCs influence O_3 formation primarily through their rapid oxidation by OH, generating peroxy radicals (RO_2), which subsequently convert NO to NO_2, promoting O_3 production [63]. However, the efficiency of this process strongly depends on the ambient NOx regime. Under NOx-limited conditions, typically found in forested and rural regions with high BVOC emissions, the availability of NOx constrains the conversion of RO_2 to NO_2, thereby limiting O_3 production efficiency despite high BVOC emissions. In contrast, under NOx-rich or VOC-limited conditions, commonly observed in urban and industrialized regions, anthropogenic emissions provide sufficient NOx to sustain efficient photochemical ozone production. This nonlinear sensitivity implies that regions with the highest BVOC-derived OFP do not necessarily correspond to the highest O_3 concentrations. Therefore, the spatial distribution of OFP should be interpreted as an indicator of theoretical sensitivity of ozone formation to BVOC emissions under high-NOx assumptions, rather than a direct proxy for ambient O_3 levels. Incorporating these photochemical mechanisms provides a more process-based understanding of the BVOC–O_3 relationship in China.

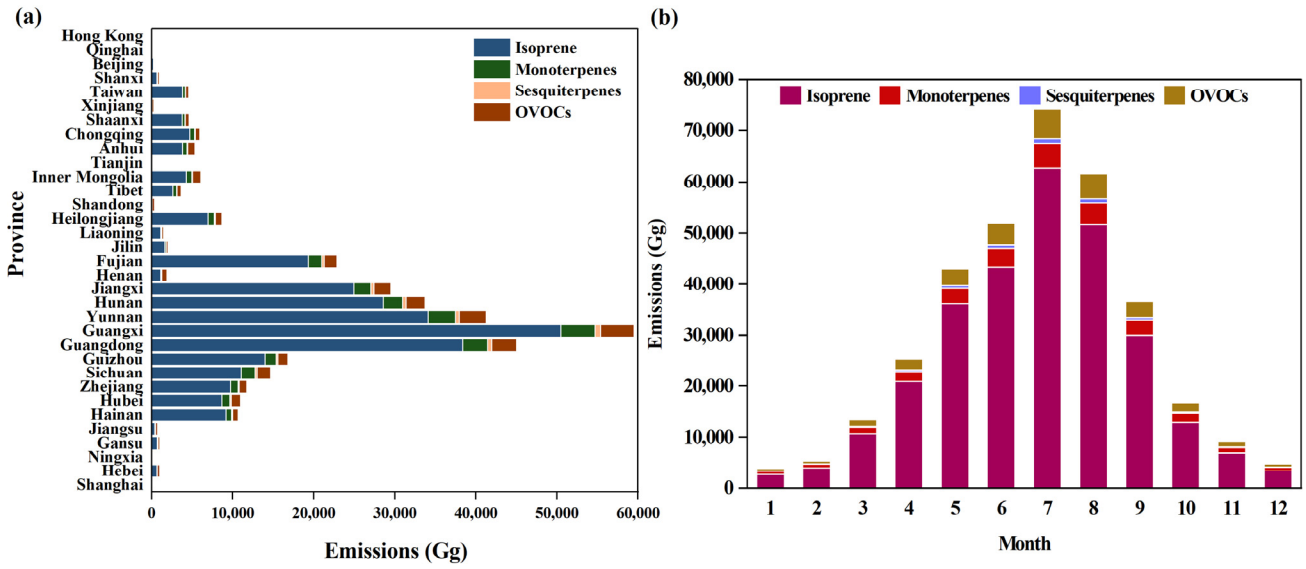

Figure 9. Provincial and seasonal variations of BVOC-driven OFP in China for 2023. (**a**) Provincial OFP; (**b**) monthly OFP.

OFP exhibits strong seasonality, following a single-peak pattern (Figure 9b). Spring, summer, autumn, and winter contribute 24%, 54%, 18%, and 4% of the annual total, respectively. Emissions peak from June to August, with July reaching 74.22 Tg (21% of the total). The lowest values occur in January–February, with January contributing only 3.86 Tg (1%). Isoprene remains the dominant contributor year-round, exceeding 80% of total OFP and peaking at 62.77 Tg in July, consistent with its strong temperature and radiation dependence. Monoterpenes and sesquiterpenes follow similar seasonal cycles, both increasing sharply in summer, reaching 4.72 Tg and 9.22 Tg, respectively, in July. OVOCs also peak in summer but show smaller amplitude, with a July maximum of 5.71 Tg. In summary, the seasonal pattern of OFP is controlled primarily by meteorological conditions and the temperature sensitivity of isoprene emissions, with monoterpenes and OVOCs making secondary contributions.

3.7. Impact on SOAFP

In 2023, the total SOAFP of BVOC emissions in China reached 2137.51 Gg yr^{-1}. Monoterpenes dominated, contributing 1488.12 Gg yr^{-1} (70% of the total), far exceeding other compound classes. This dominance reflects their high secondary organic aerosol yields (FAC = 0.18–0.5, as shown in Table S5), particularly for α-pinene (591.64 Gg yr^{-1}) and β-pinene (204.71 Gg yr^{-1}), which combine large emissions with high formation potentials. Isoprene contributed 537.94 Gg yr^{-1} (25%), limited by its low yield (FAC = 0.02) despite the largest emission mass. Sesquiterpenes accounted for 0.10 Gg yr^{-1} (5%), and though less abundant, their relatively high yields (~0.18) suggest notable regional impacts. OVOCs made minimal contributions (<1%) owing to near-zero SOA yields. The top ten species—α-pinene, isoprene, β-pinene, limonene, trans-β-ocimene, sabinene, 3-carene, myrcene, camphene, and β-caryophyllene—together contributed over 70% of the national total, confirming that SOA formation in China is primarily driven by a small set of high-yield terpenes. Importantly, while these estimates reflect potential SOA formation under constant aerosol mass assumptions, actual SOA production is influenced by the availability of anthropogenic precursors, such as NOx and pre-existing particulate matter, which can alter the oxidation pathways and reaction efficiencies of BVOCs [64].

SOAFP exhibits distinct spatial heterogeneity across China (Figure 10). High-value regions are mainly concentrated in southern China, where dense forest cover and abundant terpene emissions dominate SOA formation. Compared with OFP, SOAFP hotspots are more spatially focused, closely following forested terrain in Guangxi, Yunnan, Guangdong, Hunan, and Jiangxi, which together account for most of the national total. At the provincial scale (Figure 11a), Guangxi (341.71 Gg yr^{-1}), Yunnan (263.15 Gg yr^{-1}), and Guangdong (253.16 Gg yr^{-1}) show the highest values. Elevated SOAFP levels in these provinces result from the coexistence of coniferous monoterpene sources and broadleaf sesquiterpene emissions. In addition to the southern hotspots, notable SOAFP values also occur in the Greater and Lesser Khingan Mountains in Northeast China, reflecting the influence of extensive coniferous forests with high monoterpene yields. Provinces in Southwest China, such as Sichuan (124.75 Gg yr^{-1}), Fujian (134.69 Gg yr^{-1}), and Guizhou (106.27 Gg yr^{-1}), also exhibit substantial SOAFP due to mixed broadleaf–coniferous vegetation and favorable meteorological conditions. In contrast, northern and arid regions display very low SOAFP—for example, Beijing (1.64 Gg yr^{-1}), Tianjin (0.20 Gg yr^{-1}), Ningxia (0.14 Gg yr^{-1}), and Qinghai (0.25 Gg yr^{-1})—owing to limited forest cover and less favorable climatic conditions. Overall, SOAFP distribution highlights the crucial role of both southern and northeastern forest ecosystems in driving SOA formation across China. From a broader atmospheric chemistry perspective, SOA formation is not only controlled by BVOC emissions and local vegetation type, but also by ambient oxidant levels (OH, O_3, NO_3) and anthropogenic co-emissions, which modulate the oxidation pathways and secondary particle yields [64–66]. It should be noted that the SOAFP values presented here are calculated assuming a constant organic aerosol mass concentration, which enables comparison of relative SOA formation potential among VOC precursors. However, this simplification may underestimate SOA formation in urban or highly polluted areas, where ambient organic aerosol concentrations are typically higher [67]. Therefore, while spatial patterns emphasize the dominant role of BVOCs in southern and northeastern forested regions, the actual contribution of anthropogenic–biogenic interactions could be substantial, particularly in mixed land-use regions with high NOx and urban emissions.

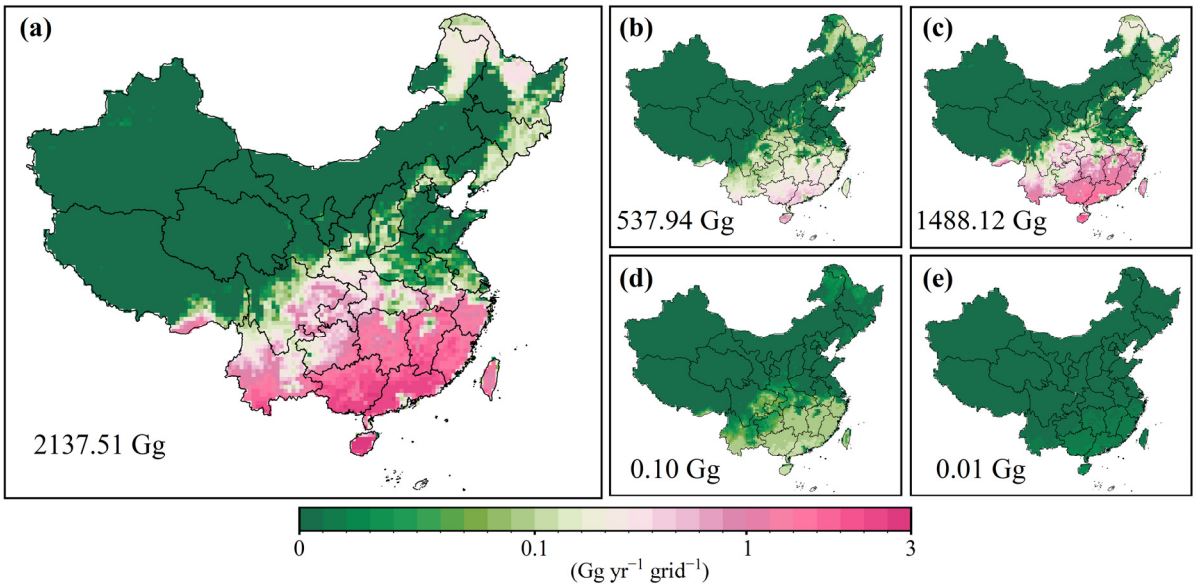

Figure 10. Spatial distribution of SOAFP from BVOC emissions in China for 2023. (**a**) Total SOAFP from BVOCs; (**b**) isoprene; (**c**) monoterpenes; (**d**) sesquiterpenes; (**e**) OVOCs.

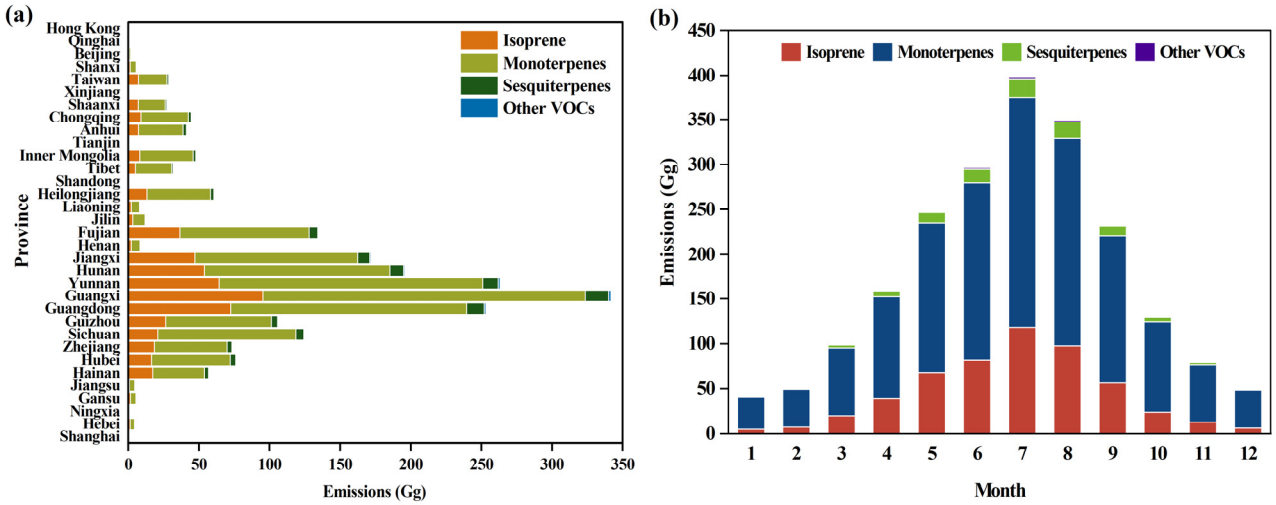

Figure 11. Provincial and seasonal variations of BVOC-driven SOAFP in China for 2023. (**a**) Provincial SOAFP; (**b**) monthly SOAFP.

Figure 11b shows that SOAFP peaks in summer (June–August) and reaches its minimum in winter, following a smoother seasonal pattern than OFP. July shows the highest monthly total, dominated by monoterpenes (256.37 Gg yr^{-1}) and isoprene (118.31 Gg yr^{-1}). Spring shows a steady increase, autumn a gradual decline, and winter remains the lowest period. Monoterpenes dominate SOAFP throughout the year, maintaining more than 70% of total formation even in winter (~40 Gg yr^{-1}). Their persistent contribution reflects both storage within vegetation and moderate temperature sensitivity. Isoprene follows a sharper, light- and temperature-driven pattern, peaking in July and dropping to ~5–7 Gg yr^{-1} in winter. Sesquiterpenes and OVOCs show similar but smaller seasonal variations. Overall, SOAFP exhibits a "summer high–winter low" cycle, but with gentler fluctuations.

3.8. Seasonal Correlation Among BVOC Emissions, OFP, and SOAFP

Figure 12 shows the monthly variations of BVOC emissions, OFP, and SOAFP in China for 2023. All three exhibit a consistent seasonal pattern, with low levels in winter and a pronounced summer peak driven by enhanced temperature, radiation, and vegetation activity. Emissions rise rapidly from spring, reach their maximum in July, and decline thereafter. In terms of magnitude, OFP overwhelmingly dominates, reaching 74.22 Tg in July, followed by BVOC emissions (8.71 Tg) and SOAFP (0.40 Tg). Although SOAFP is two to three orders of magnitude smaller than OFP, its temporal profile closely aligns with BVOC emissions, reflecting their shared biogenic source. The synchronous summer peaks across all three metrics indicate that periods of vigorous vegetation growth strengthen both photochemical O_3 production and secondary aerosol formation.

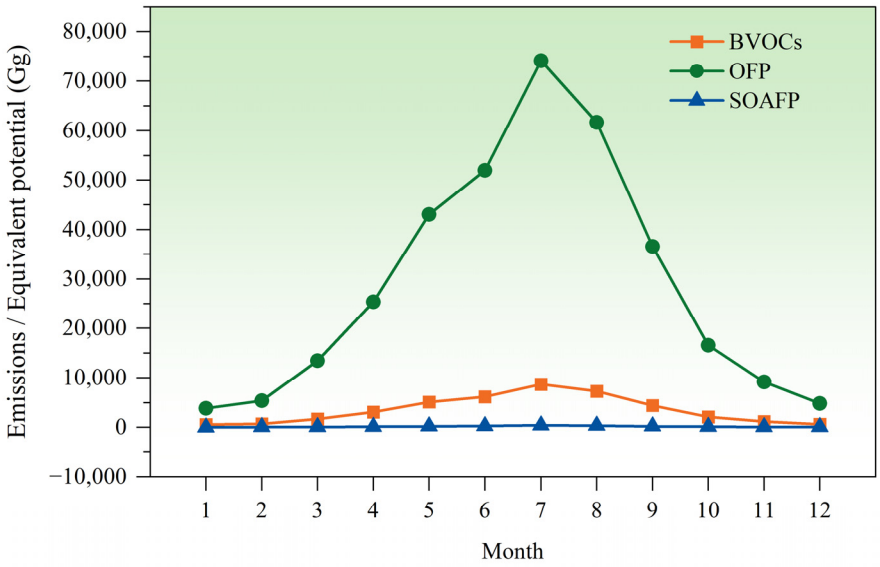

Figure 12. Monthly variations of BVOC emissions, OFP, and SOAFP in China for 2023.

SOAFP also displays a "summer-high–winter-low" pattern but with notably weaker seasonal amplitude compared with OFP. This contrast reflects fundamental chemical and physiological differences between isoprene and monoterpenes. Isoprene rapidly reacts with OH under high-temperature and high-NOx conditions, efficiently promoting O_3 formation but producing limited SOA [68]. In comparison, monoterpenes form SOA through multiple oxidants (OH, O_3, and NO_3), allowing SOA production to persist under both daytime and nighttime, and even low-NOx, environments [69]. Their oxidation also interacts with isoprene chemistry, as rapid isoprene–OH reactions can reduce the oxidant pool available for monoterpene oxidation [70]. The weaker seasonality of monoterpene-driven SOAFP is further explained by emission physiology. Isoprene emissions depend strongly on instantaneous photosynthesis, whereas monoterpenes partially originate from resin and internal storage pools, enabling release under moderate temperatures and buffering seasonal variability [52,53]. Consequently, isoprene dominates OFP, while monoterpenes disproportionately sustain SOA formation through more stable, multi-oxidant pathways. These differences highlight that O_3 and SOA formation share biogenic precursors but operate through interconnected yet fundamentally distinct atmospheric chemical mechanisms.

3.9. Uncertainty Analysis

Figure 13 shows the uncertainty in the BVOC emission inventory estimated by the MEGAN model using a Monte Carlo approach. The results indicate that the total BVOC emissions exhibit an uncertainty range of (−53%, 50%) at the 95% confidence interval.

Among individual components, the uncertainties for isoprene, monoterpenes, sesquiterpenes, and OVOCs are (−67%, 109%), (−54%, 84%), (−49%, 82%), and (−42%, 64%), respectively. Among all sources, EFs represent the dominant contributor to uncertainty across all species. EFs are described by diverse distribution types (e.g., Lognormal, Gamma, Weibull), with relatively large dispersion parameters, especially for broadleaf forests and shrublands. For instance, the lognormal distribution assigned to isoprene EF in broadleaf forests (σ = 0.66 in ln-space) implies strong right-skewness and a high probability of extreme values, which substantially enlarges the upper uncertainty bound [43]. In contrast, OVOC EFs follow normal distributions with smaller variance, resulting in more constrained uncertainty. Meteorological inputs further amplify uncertainty through nonlinear response functions in MEGAN. This effect is most pronounced for isoprene due to its high sensitivity to temperature and radiation. Activity factors further enhance uncertainty as multiplicative scalars, interacting with meteorological perturbations and reinforcing output variability. In contrast, vegetation parameters (e.g., LAI) play a secondary role due to their relatively limited variability [45]. In summary, uncertainties in emission factors, meteorological drivers, and vegetation parameters are coupled within the Monte Carlo framework, with emission factors contributing most significantly to the overall uncertainty. Future efforts should focus on improving observational constraints on emission factors, enhancing the accuracy of meteorological inputs, and optimizing model parameterizations to further reduce uncertainties and improve the reliability of BVOC emission inventories.

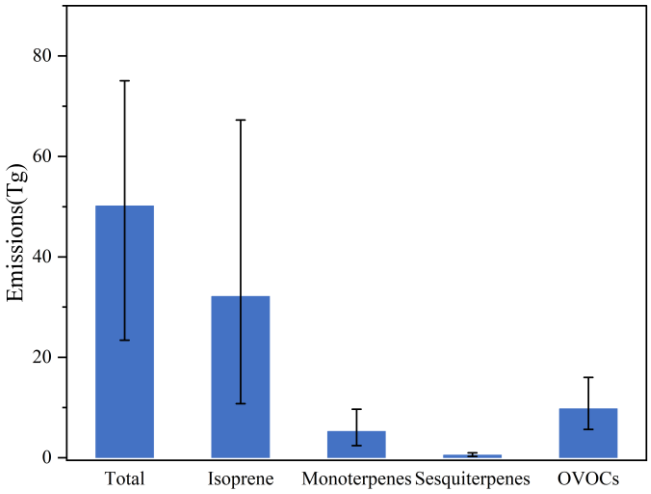

Figure 13. Uncertainty ranges of BVOC emissions derived from Monte Carlo simulations.

4. Conclusions

This study employs the MEGANv3.2 model in combination with high-resolution vegetation and meteorological datasets to construct a refined BVOC emission inventory for China in 2023 and quantitatively assesses its potential impacts on O_3 formation and SOA production. The main findings are summarized as follows. First, the inventory estimates a total annual BVOC emission of 41.70 Tg in China, with isoprene contributing the largest share (64%), followed by OVOCs (23%) and monoterpenes (12%). BVOC emissions exhibit pronounced spatiotemporal heterogeneity, with a spatial pattern characterized by "high in the south and low in the north, high in the east and low in the west," and more than 50% of the annual emissions occurring during the summer months (June–August). Broadleaf forests are identified as the dominant emission source, contributing 53% of total BVOC emissions and 75% of isoprene emissions. BVOC emissions exert significant influence on regional air quality. In terms of OFP, the total contribution from BVOCs is 346.12 Tg, with isoprene accounting for 82% due to its high emission magnitude and

reactivity. Regarding SOAFP, the total contribution is 2137.51 Gg, with monoterpenes being the primary contributors (70%), primarily driven by their high aerosol yield coefficients. Regions of high OFP and SOAFP are concentrated in forested areas of southern China, particularly in Guangxi, Yunnan, and Guangdong provinces; however, seasonal and spatial patterns differ, reflecting the distinct roles of individual BVOC species in atmospheric chemical processes.

These findings provide important implications for air quality management and policy formulation in China. The study highlights that BVOCs, particularly isoprene and monoterpenes, are key precursors for regional O_3 and SOA formation. Considering China's ongoing carbon neutrality goals and large-scale afforestation programs, which may increase vegetation cover and thereby potentially elevate BVOC emissions, future air quality management strategies should adopt a more integrated perspective [71,72]. This entails not only continued reductions of anthropogenic NOx and VOC emissions but also the incorporation of the synergistic effects of natural BVOC emissions into evaluation frameworks. Policy measures should account for the spatiotemporal distribution of BVOC emissions and their nonlinear chemical interactions with anthropogenic pollutants, with particular attention to summer ozone pollution control in southern regions with high forest cover and strong BVOC emissions. Moreover, given the significant contribution of monoterpenes to SOA formation, strategies aimed at sustained $PM_{2.5}$ reduction should emphasize monitoring monoterpene emissions in forested areas and their interactions with anthropogenic pollutants.

To advance the scientific understanding of BVOC environmental effects and support targeted management, future research should focus on several key aspects. Expanded field observations across representative vegetation types in China are essential to constrain localized emission factors and chemical speciation, thereby reducing inventory uncertainties, particularly for high-variability species such as isoprene. Integrating this inventory with regional chemical transport models (e.g., WRF-Chem, CMAQ) would enable scenario-based simulations to quantify the impacts of different carbon neutrality pathways—including afforestation types, scales, and spatial configurations—on BVOC emissions and air quality. At the same time, deeper investigation of the interactions between BVOCs and anthropogenic pollutants is needed, especially in urban clusters and downwind regions, to better resolve their respective contributions to compound pollution. In addition, coupling dynamic BVOC emission schemes with long-term climate projections would help assess the responses of emissions to changes in temperature, radiation, and CO_2 levels, thereby improving future air quality prediction and management.

Supplementary Materials: The following supporting information can be downloaded at: https://www.mdpi.com/article/10.3390/atmos17040386/s1, Table S1. Validation statistics of WRF-Simulated 2 m air temperature (T_{2m}) in 2023; Table S2. Validation statistics of downward shortwave radiation (DSR) in 2023 Derived from WRF-Simulated and the China Meteorological Forcing Dataset v2.0 (CMFD); Table S3. Comparison of annual Chinese BVOC emission with previous studies (Tg yr^{-1}); Table S4. Provincial distribution of vegetation type areas in China (km^2); Table S5. Maximum incremental reactivity (MIR) and fractional aerosol coefficient (FAC) values for BVOC species with annual emissions more than 4 Gg; Figure S1. Density scatter plot of observed and WRF-simulated T_{2m} in 2023; Figure S2. Daily area-mean DSR for 2023: WRF-simulated vs CMFD; Figure S3. MODIS PFT distribution.

Author Contributions: H.X.: Writing—review and editing, Writing—original draft, Validation, Investigation, Formal analysis, Data curation. J.Z.: Supervision, Formal analysis. Y.C.: Formal analysis. Y.Z.: Formal analysis. F.Q.: Formal analysis. H.H.: Writing—review and editing, Funding acquisition. L.F.: Writing—review and editing, Funding acquisition. D.Y.: Writing—review and editing, Supervision, Project administration, Funding acquisition. All authors have read and agreed to the published version of the manuscript.

Funding: This work was supported by the National Natural Science Foundation of China (No. 22576070), the Jing-Jin-Ji Regional Integrated Environmental Improvement-National Science and Technology Major Project (No. 2025ZD1202400 & 2025ZD1202403).

Data Availability Statement: All the data in the paper is available upon the request on the corresponding authors.

Conflicts of Interest: The authors declare no conflicts of interest.

References

1. Chaturvedi, S.; Kumar, A.; Singh, V.; Chakraborty, B.; Kumar, R.; Min, L. Recent Advancement in Organic Aerosol Understanding: A Review of Their Sources, Formation, and Health Impacts. *Water Air Soil Pollut.* **2023**, *234*, 750. [CrossRef]
2. Moses, J.A. Investigating Atmospheric Chemistry of Volatile Organic Compounds and Their Role in Climate and Air Pollution. *Int. J. Res. Publ. Rev.* **2025**, *6*, 305–328. [CrossRef]
3. Wang, P.; Zhang, Y.; Gong, H.; Zhang, H.; Guenther, A.; Zeng, J.; Wang, T.; Wang, X. Updating Biogenic Volatile Organic Compound (BVOC) Emissions with Locally Measured Emission Factors in South China and the Effect on Modeled Ozone and Secondary Organic Aerosol Production. *J. Geophys. Res. Atmos.* **2023**, *128*, e2023JD039928. [CrossRef]
4. Guenther, A.; Hewitt, C.N.; Erickson, D.; Fall, R.; Geron, C.; Graedel, T.; Harley, P.; Klinger, L.; Lerdau, M.; Mckay, W.A.; et al. A Global Model of Natural Volatile Organic Compound Emissions. *J. Geophys. Res. Atmos.* **1995**, *100*, 8873–8892. [CrossRef]
5. Guenther, A. Seasonal and Spatial Variations in Natural Volatile Organic Compound Emissions. *Ecol. Appl.* **1997**, *7*, 34–45. [CrossRef]
6. Huang, L.; Zhao, X.; Chen, C.; Tan, J.; Li, Y.; Chen, H.; Wang, Y.; Li, L.; Guenther, A.; Huang, H. Uncertainties of Biogenic VOC Emissions Caused by Land Cover Data and Implications on Ozone Mitigation Strategies for the Yangtze River Delta Region. *Atmos. Environ.* **2024**, *337*, 120765. [CrossRef]
7. Kansal, A. Sources and Reactivity of NMHCs and VOCs in the Atmosphere: A Review. *J. Hazard. Mater.* **2009**, *166*, 17–26. [CrossRef]
8. Luo, R.; Lun, X.; Gao, R.; Wang, L.; Yang, Y.; Su, X.; Habibullah-Al-Mamun, M.; Xu, X.; Li, H.; Li, J. A Review of Biogenic Volatile Organic Compounds from Plants: Research Progress and Future Prospects. *Toxics* **2025**, *13*, 364. [CrossRef]
9. Pei, D.; Wang, A.; Shen, L.; Wu, J. Research on the Emission of Biogenic Volatile Organic Compounds from Terrestrial Vegetation. *Atmosphere* **2025**, *16*, 885. [CrossRef]
10. Cao, J.; Situ, S.; Hao, Y.; Xie, S.; Li, L. Enhanced Summertime Ozone and SOA from Biogenic Volatile Organic Compound (BVOC) Emissions Due to Vegetation Biomass Variability during 1981–2018 in China. *Atmos. Chem. Phys.* **2022**, *22*, 2351–2364. [CrossRef]
11. Wu, K.; Yang, X.; Chen, D.; Gu, S.; Lu, Y.; Jiang, Q.; Wang, K.; Ou, Y.; Qian, Y.; Shao, P.; et al. Estimation of Biogenic VOC Emissions and Their Corresponding Impact on Ozone and Secondary Organic Aerosol Formation in China. *Atmos. Res.* **2020**, *231*, 104656. [CrossRef]
12. Bai, J. O_3 Concentration and Its Relation with BVOC Emissions in a Subtropical Plantation. *Atmosphere* **2021**, *12*, 711. [CrossRef]
13. Fu, C.; Xu, M. Achieving Carbon Neutrality through Ecological Carbon Sinks: A Systems Perspective. *Green Carbon* **2023**, *1*, 43–46. [CrossRef]
14. Liu, L.; Wang, X.; Wang, Z. Recent Progress and Emerging Strategies for Carbon Peak and Carbon Neutrality in China. *Greenh. Gases* **2023**, *13*, 732–759. [CrossRef]
15. Bai, G.; Kong, F.; Li, Z.; Li, L. Characteristic of Biogenic Volatile Organic Compound (BVOC) Emissions and Their Impacts on the Formation of Atmospheric Secondary Pollutants in China. *Chin. J. Ecol.* **2025**, *44*, 3694–3703. [CrossRef]
16. Cao, J. Estimation of Biogenic Volatile Organic Compound (BVOC) Emissions and Their Responses to Land Cover Changes in China During 2001–2020 Based on High-Precision Vegetation Data. Master's Thesis, Qingdao University, Qingdao, China, 2 June 2023.
17. Li, L.Y.; Chen, Y.; Xie, S.D. Spatio-Temporal Variation of Biogenic Volatile Organic Compounds Emissions in China. *Environ. Pollut.* **2013**, *182*, 157–168. [CrossRef]
18. Li, L.; Yang, W.; Xie, S.; Wu, Y. Estimations and Uncertainty of Biogenic Volatile Organic Compound Emission Inventory in China for 2008–2018. *Sci. Total Environ.* **2020**, *733*, 139301. [CrossRef]
19. Ma, M.; Gao, Y.; Ding, A.; Su, H.; Liao, H.; Wang, S.; Wang, X.; Zhao, B.; Zhang, S.; Fu, P.; et al. Development and Assessment of a High-Resolution Biogenic Emission Inventory from Urban Green Spaces in China. *Environ. Sci. Technol.* **2022**, *56*, 175–184. [CrossRef]
20. Lathière, J.; Hauglustaine, D.A.; Friend, A.D.; De Noblet-Ducoudré, N.; Viovy, N.; Folberth, G.A. Impact of Climate Variability and Land Use Changes on Global Biogenic Volatile Organic Compound Emissions. *Atmos. Chem. Phys.* **2006**, *6*, 2129–2146. [CrossRef]

21. Li, L.; Bai, G.; Han, H.; Wu, Y.; Xie, S.; Xie, W. Localized Biogenic Volatile Organic Compound Emission Inventory in China: A Comprehensive Review. *J. Environ. Manag.* **2024**, *353*, 120121. [CrossRef]
22. Zhang, B.; Jia, Y.; Bai, G.; Han, H.; Yang, W.; Xie, W.; Li, L. Characterizing BVOC Emissions of Common Plant Species in Northern China Using Real World Measurements: Towards Strategic Species Selection to Minimize Ozone Forming Potential of Urban Greening. *Urban For. Urban Green.* **2024**, *96*, 128341. [CrossRef]
23. Yin, L.; Xu, Z.; Liu, M.; Xu, T.; Wang, T.; Liao, W.; Li, M.; Cai, X.; Kang, L.; Zhang, H.; et al. Estimation of Biogenic Volatile Organic Compound (BVOC) Emissions in China Using WRF–CLM–MEGAN Coupled Model. *Biogeosci. Discuss.* **2020**, *2020*, 1–30. [CrossRef]
24. Gao, C.; Zhang, X.; Huang, L.; Yang, H.; Zhao, H.; Zhang, S.; Xiu, A. Model Intercomparisons of MEGAN and BEIS: Synergistic Impacts of Biogenic VOCs and Soil NO Emissions on Summer Ozone and Secondary Organic Aerosol Formation in China. *ACS EST Air* **2025**, *2*, 1538–1551. [CrossRef]
25. Wang, H.; Liu, X.; Wu, C.; Lin, G. Regional to Global Distributions, Trends, and Drivers of Biogenic Volatile Organic Compound Emission from 2001 to 2020. *Atmos. Chem. Phys.* **2024**, *24*, 3309–3328. [CrossRef]
26. Guenther, A.; Jiang, X.; Shah, T.; Huang, L.; Kemball-Cook, S.; Yarwood, G. Model of Emissions of Gases and Aerosol from Nature Version 3 (MEGAN3) for Estimating Biogenic Emissions. In *Air Pollution Modeling and Its Application XXVI*; Mensink, C., Gong, W., Hakami, A., Eds.; Springer Proceedings in Complexity; Springer International Publishing: Cham, Switzerland, 2020; pp. 187–192.
27. Feldner, J.; Ramacher, M.O.P.; Karl, M.; Quante, M.; Luttkus, M.L. Analysis of the Effect of Abiotic Stressors on BVOC Emissions from Urban Green Infrastructure in Northern Germany. *Environ. Sci. Atmos.* **2022**, *2*, 1132–1151. [CrossRef]
28. Feng, J.; Luo, M.; Wang, J.; Qiu, Y.; Wu, Q.; Wang, K. The influences of incorporating dynamical external forcing in WRF v3.8.1 on regional climate simulation in China. *EGUsphere* **2023**. *preprint*. [CrossRef]
29. Singh, J.; Singh, N.; Ojha, N.; Sharma, A.; Pozzer, A.; Kiran Kumar, N.; Rajeev, K.; Gunthe, S.S.; Kotamarthi, V.R. Effects of Spatial Resolution on WRF v3.8.1 Simulated Meteorology over the Central Himalaya. *Geosci. Model Dev.* **2021**, *14*, 1427–1443. [CrossRef]
30. NOAA National Centers for Environmental Information. Global Historical Climatology Network—Daily (GHCN-d). NOAA National Centers for Environmental Information. 2024. Available online: https://www.ncei.noaa.gov/products/land-based-station/global-historical-climatology-network-daily (accessed on 6 November 2025).
31. He, J.; Yang, K.; Li, X.; Tang, W.; Shao, C.; Jiang, Y.; Ding, B. China Meteorological Forcing Dataset v2.0 (1951–2024). National Tibetan Plateau/Third Pole Environment Data Center. 2024. Available online: https://cstr.cn/18406.11.Atmos.tpdc.302088 (accessed on 6 November 2025).
32. Chu, D.A.; Kaufman, Y.J.; Zibordi, G.; Chern, J.D.; Mao, J.; Li, C.; Holben, B.N. Global Monitoring of Air Pollution over Land from the Earth Observing System-Terra Moderate Resolution Imaging Spectroradiometer (MODIS). *J. Geophys. Res. Atmos.* **2003**, *108*, 4661. [CrossRef]
33. Justice, C.O.; Vermote, E.; Townshend, J.R.G.; Defries, R.; Roy, D.P.; Hall, D.K.; Salomonson, V.V.; Privette, J.L.; Riggs, G.; Strahler, A.; et al. The Moderate Resolution Imaging Spectroradiometer (MODIS): Land Remote Sensing for Global Change Research. *IEEE Trans. Geosci. Remote Sens.* **1998**, *36*, 1228–1249. [CrossRef]
34. Myneni, R.; Knyazikhin, Y.; Park, T. MODIS/Terra+Aqua Leaf Area Index/FPAR 8-Day L4 Global 500m SIN Grid V061. NASA Land Processes Distributed Active Archive Center. 2021. Available online: https://www.earthdata.nasa.gov/data/catalog/lpcloud-mcd15a2h-061 (accessed on 9 November 2025).
35. De Bock, A.; Belmans, B.; Vanlanduit, S.; Blom, J.; Alvarado-Alvarado, A.A.; Audenaert, A. A Review on the Leaf Area Index (LAI) in Vertical Greening Systems. *Build. Environ.* **2023**, *229*, 109926. [CrossRef]
36. DiMiceli, C.; Sohlberg, R.; Townshend, J. MODIS/Terra Vegetation Continuous Fields Yearly L3 Global 250m SIN Grid V061. NASA Land Processes Distributed Active Archive Center. 2022. Available online: https://www.earthdata.nasa.gov/data/catalog/lpcloud-mod44b-061 (accessed on 9 November 2025).
37. Friedl, M.; Sulla-Menashe, D. MODIS/Terra+Aqua Land Cover Type Yearly L3 Global 500m SIN Grid V061. NASA Land Processes Distributed Active Archive Center. 2022. Available online: https://www.earthdata.nasa.gov/data/catalog/lpcloud-mcd12q1-061 (accessed on 9 November 2025).
38. Gu, S.; Guenther, A.; Faiola, C. Effects of Anthropogenic and Biogenic Volatile Organic Compounds on Los Angeles Air Quality. *Environ. Sci. Technol.* **2021**, *55*, 12191–12201. [CrossRef] [PubMed]
39. Carter, W.P.L. Development of the SAPRC-07 Chemical Mechanism. *Atmos. Environ.* **2010**, *44*, 5324–5335. [CrossRef]
40. Dechapanya, W.; Russell, M.; Allen, D.T. Estimates of Anthropogenic Secondary Organic Aerosol Formation in Houston, Texas Special Issue of Aerosol Science and Technology on Findings from the Fine Particulate Matter Supersites Program. *Aerosol Sci. Technol.* **2004**, *38*, 156–166. [CrossRef]
41. Srivastava, D.; Vu, T.V.; Tong, S.; Shi, Z.; Harrison, R.M. Formation of Secondary Organic Aerosols from Anthropogenic Precursors in Laboratory Studies. *npj Clim. Atmos. Sci.* **2022**, *5*, 22. [CrossRef]
42. Lü, Z.; Hao, J.; Duan, J.; Li, J. Estimate of the Formation Potential of Secondary Organic Aerosol in Beijing Summertime. *Environ. Sci.* **2009**, *30*, 969–975. [CrossRef]

43. Zheng, J.; Zheng, Z.; Yu, Y.; Zhong, L. Temporal, Spatial Characteristics and Uncertainty of Biogenic VOC Emissions in the Pearl River Delta Region, China. *Atmos. Environ.* **2010**, *44*, 1960–1969. [CrossRef]
44. Huang, L.; Zhao, B.; He, Y.; Chang, X.; Ma, M.; Yin, D.; Wu, Q.; Wang, S. Global Wildland Fire Emissions of Full-Volatility Organic Compounds from 1997 to 2023. *Environ. Sci. Technol.* **2026**, *60*, 1965–1976. [CrossRef]
45. Situ, S.; Wang, X.; Guenther, A.; Zhang, Y.; Wang, X.; Huang, M.; Fan, Q.; Xiong, Z. Uncertainties of Isoprene Emissions in the MEGAN Model Estimated for a Coniferous and Broad-Leaved Mixed Forest in Southern China. *Atmos. Environ.* **2014**, *98*, 105–110. [CrossRef]
46. Bai, J.; Wu, Z.; Yang, C.; Guenther, A. Seasonal Variations in Whole–Ecosystem BVOC Emissions and Ozone Fluxes from a Tropical Rubber Tree Plantation in China. *Atmos. Environ.* **2025**, *351*, 121182. [CrossRef]
47. Bai, J.; Guenther, A.; Turnipseed, A.; Duhl, T. Seasonal and Interannual Variations in Whole-Ecosystem Isoprene and Monoterpene Emissions from a Temperate Mixed Forest in Northern China. *Atmos. Pollut. Res.* **2015**, *6*, 696–707. [CrossRef]
48. Bai, J.; Hao, N. The Relationships between Biogenic Volatile Organic Compound (BVOC) Emissions and Atmospheric Formaldehyde in a Subtropical Pinus Plantation in China. *Ecol. Environ. Sci.* **2018**, *27*, 991–999. [CrossRef]
49. Pacifico, F.; Harrison, S.P.; Jones, C.D.; Sitch, S. Isoprene Emissions and Climate. *Atmos. Environ.* **2009**, *43*, 6121–6135. [CrossRef]
50. Sharkey, T.D.; Monson, R.K. The Future of Isoprene Emission from Leaves, Canopies and Landscapes. *Plant Cell Environ.* **2014**, *37*, 1727–1740. [CrossRef] [PubMed]
51. Bonan, G. Importance of Leaf Area Index and Forest Type When Estimating Photosynthesis in Boreal Forests. *Remote Sens. Environ.* **1993**, *43*, 303–314. [CrossRef]
52. Guenther, A.B.; Jiang, X.; Heald, C.L.; Sakulyanontvittaya, T.; Duhl, T.; Emmons, L.K.; Wang, X. The Model of Emissions of Gases and Aerosols from Nature Version 2.1 (MEGAN2.1): An Extended and Updated Framework for Modeling Biogenic Emissions. *Geosci. Model Dev.* **2012**, *5*, 1471–1492. [CrossRef]
53. Räisänen, T. Impacts of Climate Change and Forest Management on Monoterpene Emission and Needle Secondary Compounds of Boreal Scots Pine (*Pinus sylvestris* L.). Ph.D. Thesis, University of Joensuu, Joensuu, Finland, 21 November 2008.
54. Sharkey, T.D.; Wiberley, A.E.; Donohue, A.R. Isoprene Emission from Plants: Why and How. *Ann. Bot.* **2007**, *101*, 5–18. [CrossRef]
55. Holopainen, J.K. Can Forest Trees Compensate for Stress-Generated Growth Losses by Induced Production of Volatile Compounds? *Tree Physiol.* **2011**, *31*, 1356–1377. [CrossRef]
56. Shan, Y.; Jin, S. Biosynthetic Machinery to Abiotic Stress-Driven Emission: Decoding Multilayer Regulation of Volatile Terpenoids in Plants. *Antioxidants* **2025**, *14*, 673. [CrossRef]
57. Liu, Y.; Ciuraru, R.; Abis, L.; Amelynck, C.; Buysse, P.; Guenther, A.; Heinesch, B.; Lafouge, F.; Levavasseur, F.; Loubet, B.; et al. Emissions of biogenic volatile organic compounds from agricultural lands and the impact of land-use and other management practices: A review. *EGUsphere* **2024**. *preprint*. [CrossRef]
58. Li, L.; Zhang, B.; Cao, J.; Xie, S.; Wu, Y. Isoprenoid Emissions from Natural Vegetation Increased Rapidly in Eastern China. *Environ. Res.* **2021**, *200*, 111462. [CrossRef]
59. Dudareva, N.; Klempien, A.; Muhlemann, J.K.; Kaplan, I. Biosynthesis, Function and Metabolic Engineering of Plant Volatile Organic Compounds. *New Phytol.* **2013**, *198*, 16–32. [CrossRef]
60. Duhl, T.R.; Helmig, D.; Guenther, A. Sesquiterpene Emissions from Vegetation: A Review. *Biogeosciences* **2008**, *5*, 761–777. [CrossRef]
61. Malik, T.G.; Sahu, L.K.; Gupta, M.; Mir, B.A.; Gajbhiye, T.; Dubey, R.; Clavijo McCormick, A.; Pandey, S.K. Environmental Factors Affecting Monoterpene Emissions from Terrestrial Vegetation. *Plants* **2023**, *12*, 3146. [CrossRef] [PubMed]
62. Ma, W.; Feng, Z.; Zhan, J.; Liu, Y.; Liu, P.; Liu, C.; Ma, Q.; Yang, K.; Wang, Y.; He, H.; et al. Influence of Photochemical Loss of Volatile Organic Compounds on Understanding Ozone Formation Mechanism. *Atmos. Chem. Phys.* **2022**, *22*, 4841–4851. [CrossRef]
63. Tan, Z.; Lu, K.; Jiang, M.; Su, R.; Dong, H.; Zeng, L.; Xie, S.; Tan, Q.; Zhang, Y. Exploring Ozone Pollution in Chengdu, Southwestern China: A Case Study from Radical Chemistry to O3-VOC-NOx Sensitivity. *Sci. Total Environ.* **2018**, *636*, 775–786. [CrossRef] [PubMed]
64. Kelly, J.M.; Doherty, R.M.; O'Connor, F.M.; Mann, G.W. The Impact of Biogenic, Anthropogenic, and Biomass Burning Volatile Organic Compound Emissions on Regional and Seasonal Variations in Secondary Organic Aerosol. *Atmos. Chem. Phys.* **2018**, *18*, 7393–7422. [CrossRef]
65. Shilling, J.E.; Zaveri, R.A.; Fast, J.D.; Kleinman, L.; Alexander, M.L.; Canagaratna, M.R.; Fortner, E.; Hubbe, J.M.; Jayne, J.T.; Sedlacek, A.; et al. Enhanced SOA Formation from Mixed Anthropogenic and Biogenic Emissions during the CARES Campaign. *Atmos. Chem. Phys.* **2013**, *13*, 2091–2113. [CrossRef]
66. Palm, B.B.; Campuzano-Jost, P.; Day, D.A.; Ortega, A.M.; Fry, J.L.; Brown, S.S.; Zarzana, K.J.; Dube, W.; Wagner, N.L.; Draper, D.C.; et al. Secondary Organic Aerosol Formation from in Situ OH, O_3, and NO_3 Oxidation of Ambient Forest Air in an Oxidation Flow Reactor. *Atmos. Chem. Phys.* **2017**, *17*, 5331–5354. [CrossRef]

67. In 'T Veld, M.; Khare, P.; Hao, Y.; Reche, C.; Pérez, N.; Alastuey, A.; Yus-Díez, J.; Marchand, N.; Prevot, A.S.H.; Querol, X.; et al. Characterizing the Sources of Ambient PM10 Organic Aerosol in Urban and Rural Catalonia, Spain. *Sci. Total Environ.* **2023**, *902*, 166440. [CrossRef]
68. Steiner, A.L. Role of the Terrestrial Biosphere in Atmospheric Chemistry and Climate. *Acc. Chem. Res.* **2020**, *53*, 1260–1268. [CrossRef]
69. Zhang, H.; Yee, L.D.; Lee, B.H.; Curtis, M.P.; Worton, D.R.; Isaacman-VanWertz, G.; Offenberg, J.H.; Lewandowski, M.; Kleindienst, T.E.; Beaver, M.R.; et al. Monoterpenes Are the Largest Source of Summertime Organic Aerosol in the Southeastern United States. *Proc. Natl. Acad. Sci. USA* **2018**, *115*, 2038–2043. [CrossRef]
70. Schervish, M.; Heinritzi, M.; Stolzenburg, D.; Dada, L.; Wang, M.; Ye, Q.; Hofbauer, V.; DeVivo, J.; Bianchi, F.; Brilke, S.; et al. Interactions of Peroxy Radicals from Monoterpene and Isoprene Oxidation Simulated in the Radical Volatility Basis Set. *Environ. Sci. Atmos.* **2024**, *4*, 740–753. [CrossRef]
71. Liu, S.; Sahu, S.K.; Zhang, S.; Liu, S.; Sun, Y.; Liu, X.; Xing, J.; Zhao, B.; Zhang, H.; Wang, S. Impact of Climate-Driven Land-Use Change on O3 and PM Pollution by Driving BVOC Emissions in China in 2050. *Atmosphere* **2022**, *13*, 1086. [CrossRef]
72. Gai, Y.; Sun, L.; Fu, S.; Zhu, C.; Zhu, C.; Li, R.; Liu, Z.; Wang, B.; Wang, C.; Yang, N.; et al. Impact of Greening Trends on Biogenic Volatile Organic Compound Emissions in China from 1985 to 2022: Contributions of Afforestation Projects. *Sci. Total Environ.* **2024**, *929*, 172551. [CrossRef]